Silicon (2023) 15:6085–6097
https://doi.org/10.1007/s12633-023-02486-4

RESEARCH

Stress Engineering of a Window Porous Silicon Layer based on Pseudo Substrate Suitable for III-V Monolithic Integration

Aicha Saidi[1] · Imen Zeydi[1] · Badreddine Smiri[1,2] · Isabelle Berbezier[3] · Ridha Mghaieth[1]

Received: 23 February 2023 / Accepted: 19 April 2023 / Published online: 8 May 2023

Abstract
Due to Silicon (Si) material abundance and specific properties, monolithic integration of III-V semiconductors on (Si) is of paramount importance for the next-generation in Optoelectronic devises. An alternative approach to lattice mismatched single silicon crystal substrates for heteroepitaxy is proposed. In this work, we have suggested a design of a compliant virtual substrate and we have explored the modulation of stress/lattice parameter of a window layer based on porous silicon pseudo-substrates allowing a defect free epitaxial growth. We prepared a silicon window layer with low porosity and variable thicknesses whose stress is modulated by the succession of several layers with gradual porosity. As a result, we evaluated the stress and the lattice parameter in compliant substrate before and after thermal annealing. The pores reorganization process was supported in Argon atmosphere at constant temperature (900 °C). The samples were studied morphologically by Field Emission scanning Electron Microscope (FE-SEM) and structurally by High Resolution X-Ray Diffraction (HR-XRD) and Nano-Raman.

Keywords Porous silicon · Window layer · Tensile strain · Thermal annealing · HR-XRD · Nano-Raman spectroscopy

1 Introduction

Microelectronics industry based on Silicon has attracted a great attention due to its discriminate structural and electrical features. Nowadays, a significant amount of research has arisen in the synthesis and application of its porous derivative. Since the discovery of porous silicon, several functionalities in different fields have been investigated, for instance: solar cells, biomedical application [1], sensors [2, 3] and photodetector devices [4]. Porous silicon has been approved like a key material for microelectronics as a sacrificial layer or as a fundamental structural material due to its flexible physical and morphological qualities. Its sponge structure infused a quit vast internal surface area and a highly chemical reactive that can touch optical, thermal, electrical and mechanical properties. The recent developments, where the technology dimensions are shrunk, require the control of stress in structures and thereupon seeking its origins.

Porous silicon is made from electrochemical anodization of silicon in HF solution. It is an advantageous method thanks to its simplicity although the great number of implicated parameters in the formation of porous structures [5]. Current densities, etching duration, HF concentration, doping type and temperature are indispensable factors that affect this spongy structure.

The aim of this study is to prepare the porous silicon to the monolithic integration of III-V compound semiconductors. This approach was and still one of the pertinent strategies to overcome the lattice mismatch, polarity difference and thermal expansion mismatch between those two materials, in order to reduce the formation of high density of dislocation in the epitaxial layer [6]. Such technique uses porous silicon as a compliant substrate to adapt stress in the epitaxial layer through the deformation of porous silicon. In the present contribution, series of porous silicon layers were fabricated in three stages starting by generating a low porosity thin layer on a higher porosity one by varying the current densities to modify the degree of porosity. Controlling anodization time defines each layer thickness. Then applying high temperature treatment in non-oxidized gas to

✉ Imen Zeydi
imenzeydi11@gmail.com

[1] Laboratoire Micro-Optoélectroniques Et Nanostructures (LR99ES29), Faculté Des Sciences de Monastir, Université de Monastir, Avenue de L'environnement, 5019 Monastir, Tunisie

[2] LPCNO, INSA-CNRS-UPS, Université de Toulouse, 31077 Toulouse, France

[3] Institut Matériaux Microélectronique Nanoscience de Provence, UMR CNRS 6242, Aix-Marseille Université, 13997 Marseille, France

close the top porous silicon layer and reorganize the other pores in the structures. At the end, the top surface changes into a quasi-defect-free crystalline layer convenient for an epitaxial growth.

In this paper, to evaluate the different structures, Filed Emission scanning Electron Microscope FE-SEM, X-Ray Diffraction and Nano-Raman are proposed to study the lattice mismatch between the different porous layers and the bulk. Gradient porosity, thermal annealing and stress have to be taken into consideration to analyze lattice parameter expansion.

2 Experimental

Samples were fabricated from heavily p-doped silicon substrate (p +), ~ 0.01 Ω.cm resistivity, (100) orientation and 380 µm thickness. Due to the high chemical affinity in their surface, a cleaning process was primordial before and after the anodization step in order to obtain homogeneous porous surface. The silicon (Si) wafers were connected to anode and gold to cathode in a Teflon cell. The wafer was electrochemically anodized using a mixture of HF (48%) and Ethanol (HF:C_2H_5OH 1:0.6) in the darkness which allows to obtain a low porosity rate. The HF mixture was preserved for samples fabrication while varying the current density and the anodization time. Just after the fabrication of the porous structures, the samples were rinsed in deionized water (18 MΩ), then dried under a nitrogen gas flow to remove any trace of electrolyte. The samples were placed in a vacuum desiccator to avoid possible native oxidation. Porous silicon mono-layer (PS1, PS2) and porous silicon multi-layer (PSML1, PSML2) stacks were etched in galvanostatic mode using various current densities and etching duration as shown in Fig. 1.

Afterward, our samples were annealed (PS1R, PS2R, PSML1R and PSML2R) in tubular furnace Nabertherm B400 series (ceramic: Pythagoras C610) by gas (Argon or Nitrogen) circulation at 900 °C with 270 °C/hour heating rate in 300 mbar and with a flow rate of 200L/hour for a constant duration.

Pore diameter and porous thickness were analyzed using Gemini SEM 500 (FE-SEM), which was equipped with an ideal detector "In-lens" for displaying the surface structures. The images were acquired at low electron acceleration voltage in order to obtain a high resolution nanoscopic structures. The aim was to investigate the evolution in the crystalline structures after each process (anodization, annealing treatment) to estimate the effect on lattice mismatch. The HR-XRD experiments were performed with D8 DISCOVER Bruker Axis Diffractometer operated in the four-axis with monochromatic CuKα1 radiation at 1.54060 Å. This technique was operated on ω-2θ on (004) reflection. The sensitivity of this mode to the lattice mismatch involves the strain in the perpendicular direction. HR-XRD can also be operated by rocking curve to induce the tilt. Raman Spectroscopy, as a non-destructive technique, allows the characteristic elements vibrations with 532 lasers through LabRAM HR Evolution Raman microscope of HORIBA with diffraction gratings of 300 gr/mm. A microscope objective (X100) focused the incident laser beam, about 633 nm to a spot diameter about 100 microns onto the sample surface. The spectra were obtained in a back scattering using 521 cm^{-1} bond of virgin silicon wafer.

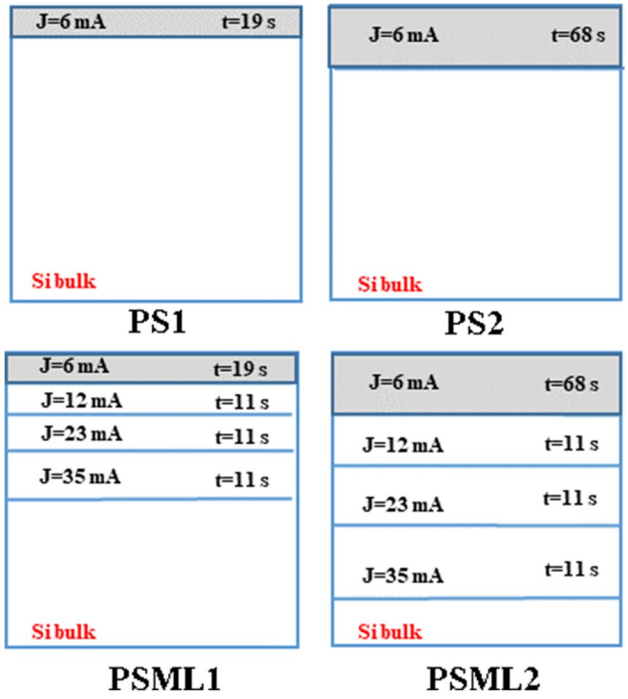

Fig. 1 Schematic representation of the investigated samples

3 Result and Discussion

3.1 The Effect of Etching Conditions on Porous Layers Structures

After etching, samples were characterized using Filed Emission scanning Electron Microscope. FE-SEM is commonly employed for analyzing the structures porosity. Information such pores geometry, shapes, pore distribution on the depth can be delivered especially for mesoporous silicon. Cross-section micrographs show a discriminant view of the porous layer, which is distinguished from the substrate. As a result, for porous silicon monolayer (PS), increasing the anodization time increases the porous silicon thickness from 0.35 µm to 0.70 µm (Fig. 2).

On the other hand, for porous silicon multilayers (PSML), at high magnification, it can be observed that the contrast

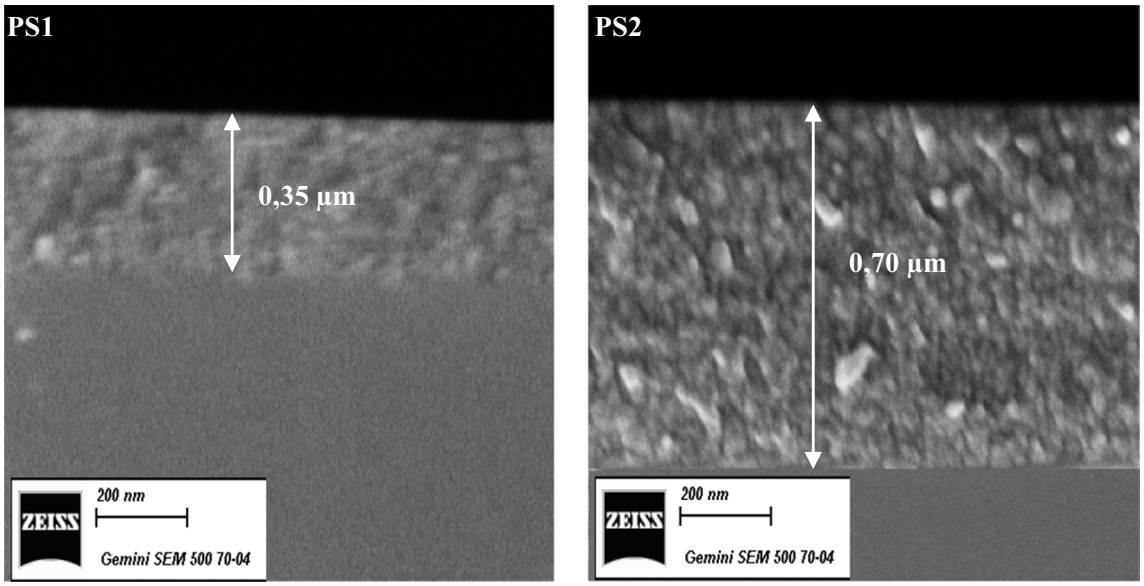

Fig. 2 FE-SEM image cross sections: porous silicon monolayer (PS): PS1 and PS2

depends on the porosity gradient of each layer. Thereby, the thickness of different multilayers can be measured. The following thicknesses were determined as shown in (Fig. 3a, a'). Even-though, the same anodization conditions were maintained constant in the bottom layers (the three high porous layers (HPLs) with different variant current densities) during the etching process, we have found that the thickness of these porous layers were different. Within the set of analyzed value, the electrolyte can easily pass through the upper porous layer without interacting with the pore wall [7]. The two structures exhibit a channel encircled by a skeleton of crystalline silicon nanowires (Fig. 3b), they lie along the (001) direction perpendicular to the bulk surface where the pores per se are extensively ramified and show a very characteristic "fir-tree'' which is called in other works a dendritic geometry [8].

Prior research [9] suggests that average pores diameter between 2 and 50 nm are assigned as mesoporous silicon.

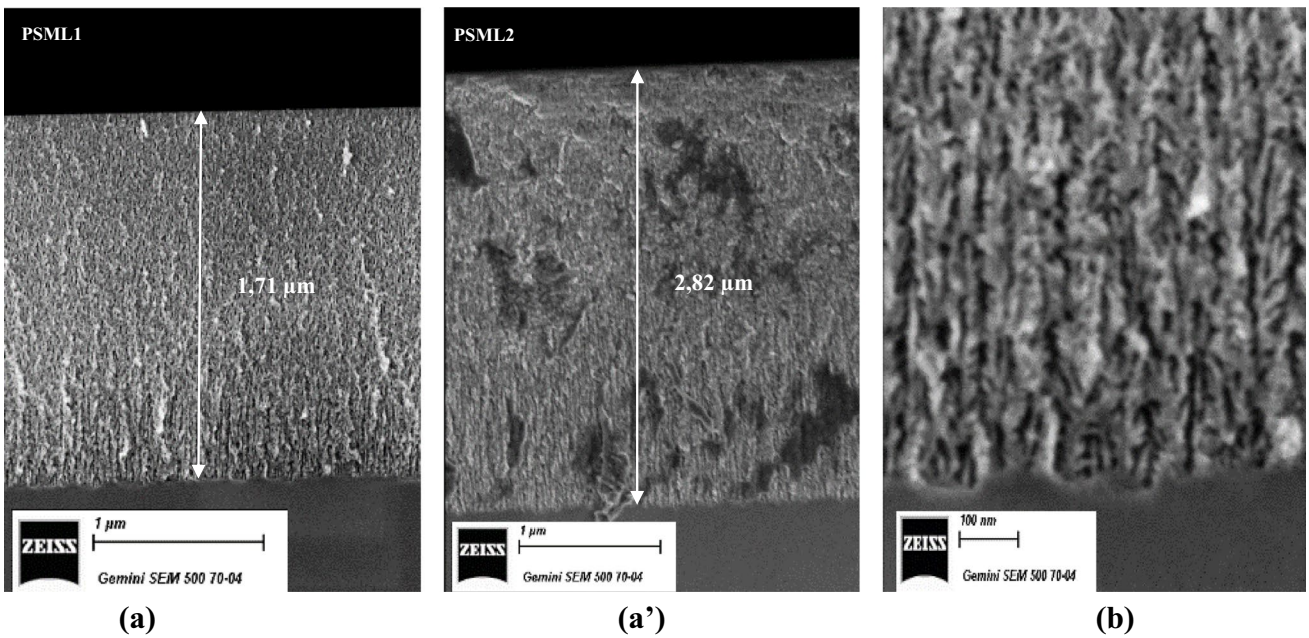

Fig. 3 FE-SEM cross section images of porous silicon multilayers pre-annealing: **a** PSML1, **a'** PSML2, **b** interface porous silicon/ silicon

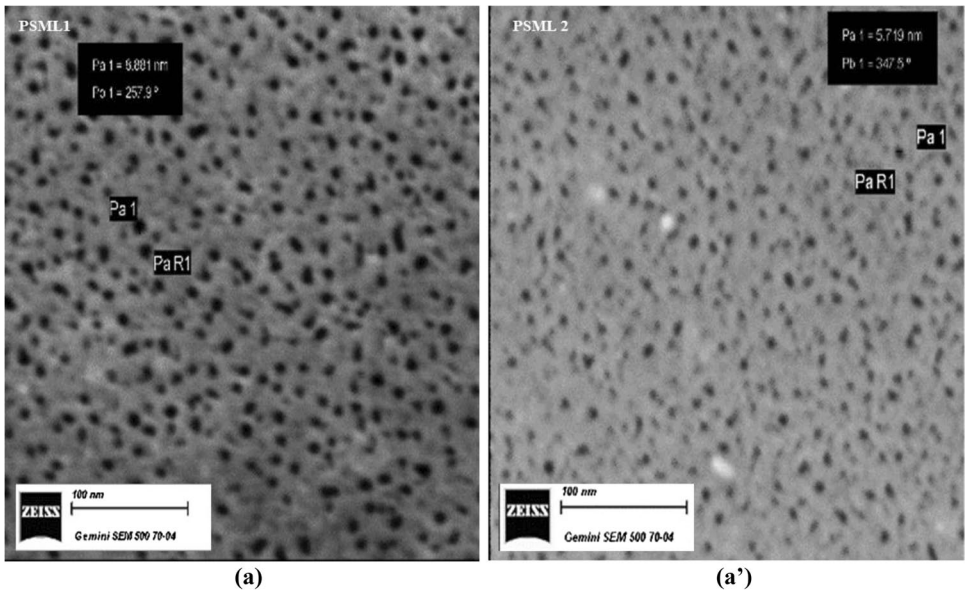

Fig. 4 FE-SEM top view images of porous silicon multilayers pre-annealing: **a** PSML1, **a'** PSML2

For this study, the average pore size, obtained from (Fig. 4a, a'). was around 7.3 nm. From the image J software, we can estimate the vacancy ratio on the top surface layer of each multilayer sample. The applied procedure consists in dividing the total coverage area of pores by the image area. The obtained values were 11.32% (PSML1) and 15.75% (PSML2) respectively, which allows obtaining a notable silicon area, with modified lattice parameters, suitable for molecular beam epitaxy growth of III-V on silicon. Taking altogether, this outcome demonstrates the second effect of anodization time: an increasing in anodization time can generate a higher porosity provided with slightly expanded pores [10].

3.2 Post Annealing

The significant feature of silicon manifests in its extreme sensitivity to heat. The samples were annealed at 900 °C where Argon was carried out for 30 min. The heat treatment engenders a main change in pores details: size and distribution (Fig. 5a, b). As with prior works, the argon annealing process served in obtaining an upper surface almost pores free which witnesses the formation of quasi-monocrystalline layer. The driving force of this process is the reduction of surface energy. In fact, the thermal process is an approach to rearrange the voids, which are covered by the theory of sintering. High temperature Argon annealing split off the

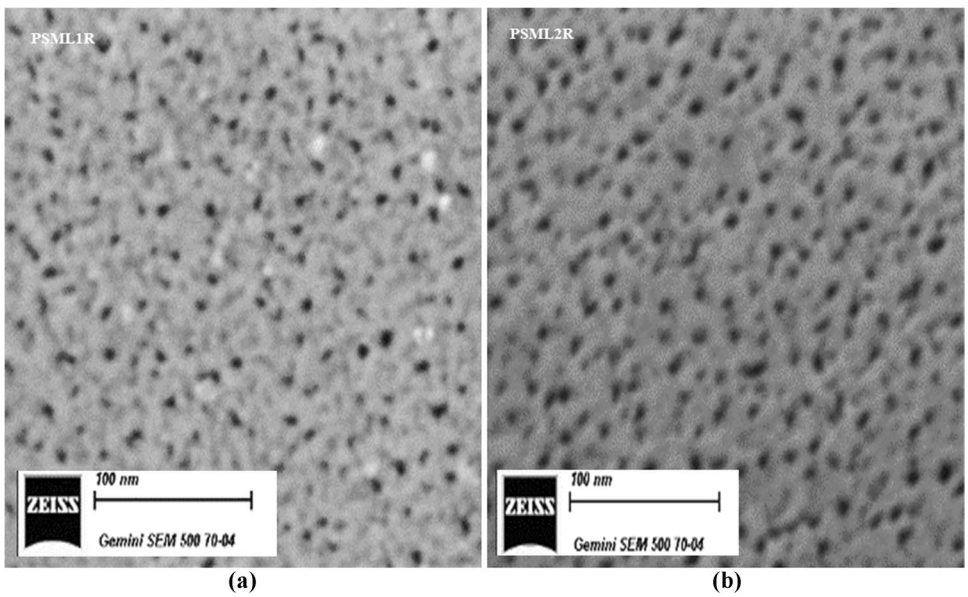

Fig. 5 FE-SEM top view image of porous silicon multilayer post-annealing at 900 °C for 30 min:**a** PSML1R, **b** PSML2R

Table 1 The variation of pores air and densities in multilayers porous structures pre-and post-annealing

Structures		Image J software	
		Pre-annealing	Post-annealing
average pores air (nm^2)	PSML1	68.80	42.12
	PSML2	78.55	61.42
Average pores density (pores/μm^2)	PSML1	1646	1230
	PSML2	2005	1568
Vacancy ratio	PSML1	11.32%	5.18%
	PSML2	15.75%	9.63%

Si–H bonds fixed on the surface of the pore walls during etching process.

Whereas PSMLs show strong interaction leading to pores shrinkage in the starting layer and simultaneous coalescence of pores population in the bulk. The void coalescence mechanism consists in top-down migration of pores from the layer with the lowest porosity rate to layers with the highest porosity density causes a diminution in the pores air respectively in the pores densities as listed in Table 1.

The different layers can be clearly distinguished in Fig. 6a. At the interface with the silicon substrate this process stops. This was explained by the Ostwald ripening process that occurs in the lower porous layers [7]. Since the vacancy concentration in the upper layer is higher than the bulk, a vacancy diffusion appears from the starting layer to the interface porous silicon/silicon signifying that high vacancy gradient mainly depends on the porosity difference [11]. Since the presence of hydrogen atoms near the free surface of PSi introduces a pre-deformation in the silicon lattice, during the heating process at 900 °C, the silicon crystallites begin to plastically deform producing a nonlinear deformation (elastic + plastic). The displacements and the loads imposed on the boundary of the structures induce a stress field inside the matrix. Under the effect of the pores migration, the external loads applied to the material induce the deformation or modification of the dimensions of the material. As the porosity is low, the crystalline structures present a sufficient resistance to dissection and do not preserve the original shapes.

To explain the deformation process, we use a scheme developed from observations on the edge of a multilayer structure Fig. 6b. During the annealing operation, the pores migrate from the window layer to the lower layers. Thus, a lateral deformation is obtained in the volume of the porous matrix. Pore enlargement in the layer at the interface with the substrate induces a compressive deformation in the crystals surrounding the pores. Due to porosity gradient decrease from bottom to top, a stress gradient then occurs in the perpendicular direction at the origin of the deformation of the crystalline cell along the axis perpendicular to the surface.

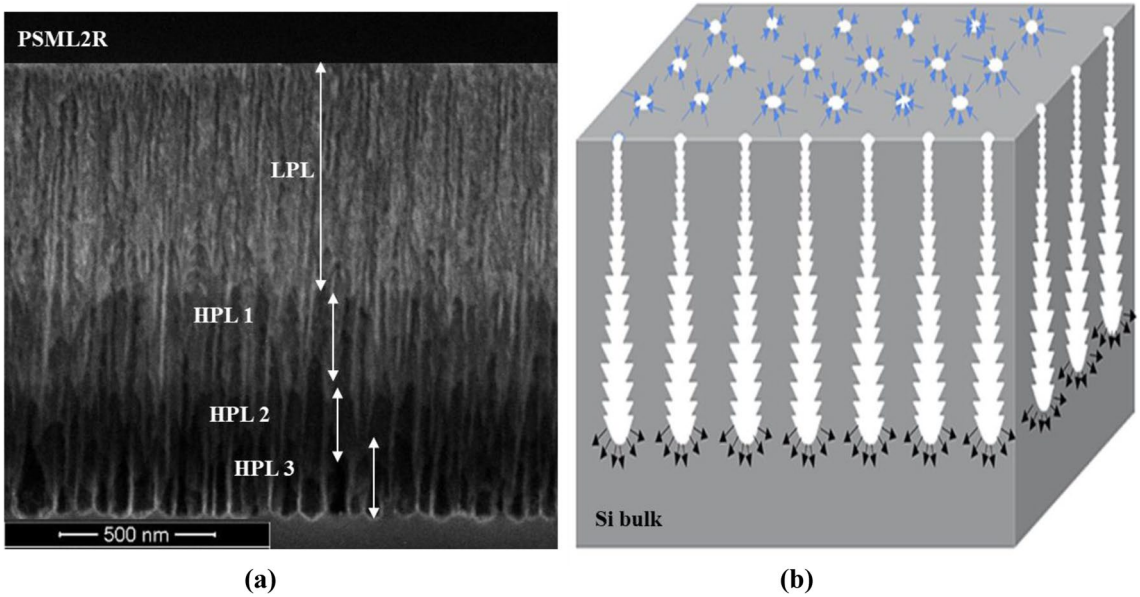

Fig. 6 **a** FE-SEM cross section image of porous silicon multilayer PSML2R post-annealing at 900 °C for 30 min, **b** schematic representation of the pore's redistribution and the evolution of the stress after annealing

This results in a second effect, which contributes to the pores closing process.

3.2.1 Porous silicon monolayer

- Pre-annealing treatment:

In order to further evaluate the crystallinity of samples, HR-XRD was analyzed in room temperature. As sketched in Fig. 7 (plotted on semi logarithmic scale), XRD profiles of porous silicon monolayer (PS) show three distinct Bragg diffractions: the main peak is attributed to the monocrystalline silicon substrate since the X-ray was recorded at the (400) reflection from the lattice planes parallel to the (100) silicon surface. While the shoulder peak on the left is related to the sintered porous silicon layer. This peak is a result of the lattice expansion in the z direction [12]. On account of the time analysis, a third peak on the right side appears and it was referred to $K_{\alpha 2}$. A review of the literature shows that the relative height of these peaks (except for the $K_{\alpha 2}$ peak) is determined by the thickness, density and crystalline quality of the porous film, thence an increase in any of these parameter will increase the magnitude of the porous film diffraction peak [13]. In some of the very low-density samples, no diffracted peaks from the porous film were observed above the background signal [12].

Upon anodization, the porous silicon peak shifts to a lower angle relative to silicon peak. Such behavior indicates that the lattice parameter of the porous silicon matrix is expanded with respect to the substrate, therefore, in the case of a single porous layer, the PS layer stretches along the [100] direction. The expansion of the lattice parameter is ascribable to the substitution of the Si crystallites surface by Si-H_x. This mechanism is known under the name of liquid physisorption: in-point-of-fact, when silicon sample is totally covered with HF solution, the oxide evanesces and the pore walls adsorb a high density of hydrogen. Si-H_x bonds produce in-plane compressive strain of the pore side walls. The stress leads to an out-plane expansion of the PS lattice resulting in the out of plane tensile strain [14]. The perpendicular strain relative to each distribution can be calculated using Bragg's Eq. (1) [15]:

$$\varepsilon_T : -\Delta\theta/tg\theta \quad (1)$$

Where $\Delta\theta$ the angular separation between PS and Si substrate is peaks and θ is the Bragg diffraction angle. The different values of perpendicular strain calculated for pre- and post-annealing structures are summarized in Table 2.

Regarding the splitting between the two peaks ($\Delta\omega$), it increases according the PS monolayer thickness. Our results show an incremental increase about 13.6% in the tensile strain. Referring to Barla et al., there is a correlation between porosity and strain: they found a linear increase in the lattice parameter expansion for p + type doped PS films, the strain ε_T increases from 3 to 8×10^{-4} when the porosity increases from 30 to 80% [16]. The difference in strain values between PS1 and PS2 structures is attributed to the existence of different preferential distribution of crystallites sizes formed during the anodization process [17].

- Post-annealing treatment:

In order to reorganize the surface, heat treatment at high temperature was required (900 °C for 30 min for all samples),

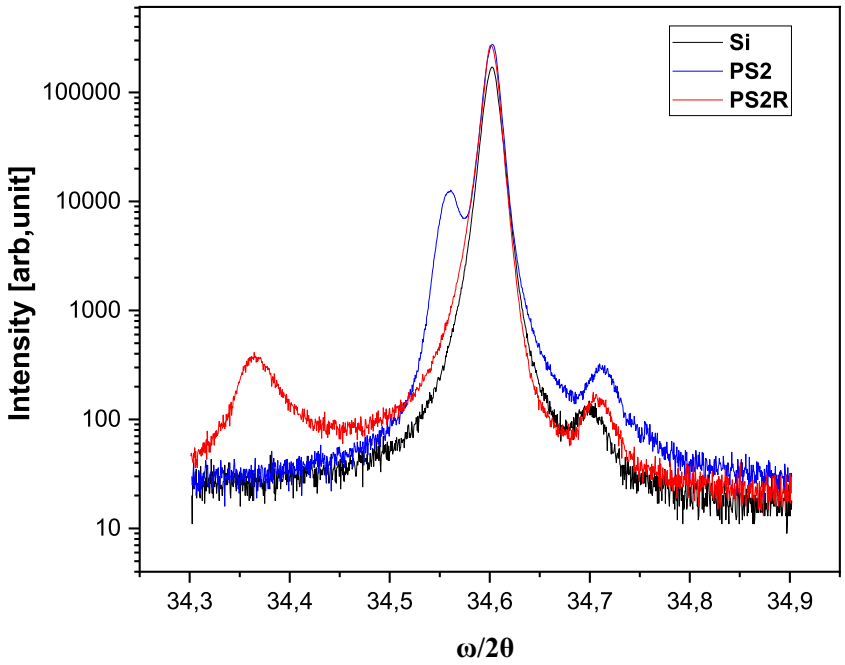

Fig. 7 High Resolution XRD profiles of porous silicon monolayer (PS): pre-anodization process

Table 2 Peak separation in ω-2θ scan and the calculated perpendicular lattice strain in monolayer porous silicon (PS) pre-and post-annealing treatment

Structures	θ_{Ps}	$\Delta\omega = \theta_{Si}-\theta_{Ps}$	$(\Delta d/d)$ [10^{-4}]
PS1	34.564	-0.039	4.9
PS2	34.559	-0.044	5.57
PS1R	34.480	-0.125	15.59
PS2R	34.365	-0.238	30.1

thus and so the top layer with low porosity becomes quasi-pores free. The sintered porous peaks shift even more to lower angles as shown in Fig. 8a, b indicating the relaxation of the PS lattice parameter to the value of monocrystalline Si. Actually, the tensile strain is ascribed to the porosity increase in the bottom layers under the influence of temperature.

Compared to anodized samples (PS1 and PS2); heat treatment caused a radical change in monolayer structures. The diffraction porous peaks shift indicates that there is an inhomogeneous strain distribution inside the crystallite material. At this point, it is noteworthy to mention that due to thermal annealing, voids reorganization occurs through vacancy diffusion process known as pores coalescence. Pores therefore migrate from the low porosity layer to the higher one and grow in the parallel direction respectively helping to relieve more stress. This result was reported in FE-SEM measurements.

We assume that the silicon crystallites are deformed due to a distribution in-plane tensile strain caused by the enlargement of the pores in the bottom layer, which leads to an expansion of the perpendicular and parallel lattice parameter of the window layer.

3.2.2 Porous Silicon Multilayer

- Pre annealing treatment:

The purpose of adding high porosity layers under the low porosity one is the ability to modulate the strain: in this case, the lower stressed crystallites of the window layer will help the relaxation of the higher stressed matrix of the high porosity layers through their interface. Two types of PSML were prepared by appending three gradual high-porosity layers under the window layers as mentioned earlier. Three sharp diffraction peaks appeared (Fig. 9(a)); since the crystallinity of porous layers mainly depends on the anodization current control, HR-XRD profiles should exhibit more distinct diffraction peaks, which are typical patterns of each porous layer interface. In our case, since the variation of anodization current density from one layer to another is quite short, the chosen anodization time does not create a clear interface between them. The peak positions indicate the presence of two tensile strained layers. This result suggests the presence of a strain distribution inside the crystallites, which depends on their size. The shoulder peak corresponds to crystallites with larger dimensions, which are under less strain and could be fitted with a Voigt distribution similar to the bulk Si. The other peaks are related to smaller crystallites which are more stressed [17]. By using the angle at peak intensity and the angle separation between the two peaks (Δω), the average internal stress of multilayer porous structures pre-and post-annealing was calculated as shown in Table 3, which is approximately two times higher than the first porous peak. We can assume that these differences in strain can be associated to the etching condition confirmed by FE-SEM observations.

Regarding the diffraction intensity at very lower angles, the diffraction peak in PSML1 is higher than the one in PSML2. The total thickness of HPL in PSML1 and PSML2 are prepared under the same conditions, even though XRD spectra reveal different diffraction in terms of intensities. This result can be explained by the fact that the thickness of the top layers in both structures are different [18].

- Post-annealing treatment:

Specimens were annealed in Argon atmosphere at 900 °C for 30 min, which results, as discussed above, the sintering of the porous layer: tiny voids seal and the low porosity layer become quasi-crystalline forming a split plane in high

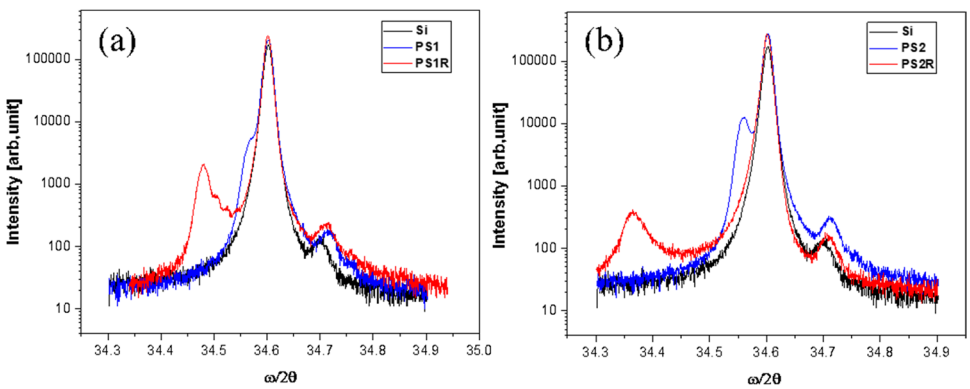

Fig. 8 High Resolution XRD profiles of porous silicon monolayer (PS): **a** PS1 post-annealing, **b** PS2 post-annealing

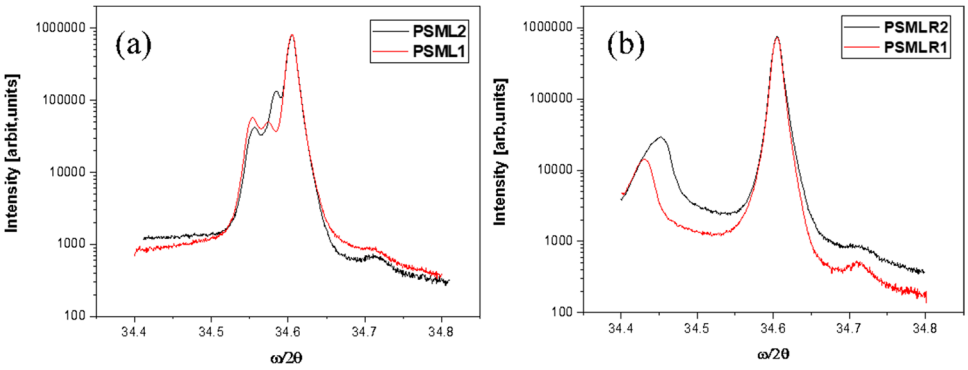

Fig. 9 High Resolution XRD profiles of porous silicon multilayer (PSML): **a** pre anodization process, **b** upon annealing

porosity layers. We may expect pores bending by allowing a strain relief. This result evidences that pores reorganization produces an expansion of the perpendicular and parallel lattice parameter of each porous silicon layer. This behavior is also applicable for the window layer. We can then evince the possibility of modulating the stress of the window layer by using embedded porous layers.

XRD profiles (Fig. 9b) depict one diffracted peak of porous silicon, which indicates voids reorganization in the two different patterns (interfaces). After annealing, the material movement vanishes the clear interfaces, which explains the appearance of a single diffraction peak. However, according to FE-SEM observations the variation in porosity is continuously gradual. Then, we can suggest that the strain in PSML1 is higher than the one in PSML2 which is explained by the fact that when the thickness of the window layer increases, a higher force is exerted on the HPLs, helping their coalesced pores to relieve more stress [14].

3.3 Raman

Nano Raman measurements have been employed to investigate the change of atomic spacing and strain induced through analyzing the lattice vibration and their adjustments after each process (anodization, thermal annealing…). The phonon modes of silicon are divided as longitudinal optical phonons (LO) and transverse optical phonons (TO). This classification depends primordially on the surface of porous silicon which scattering data are observed; according to the Raman selection rules in a silicon semiconductor, only scattering by LO phonon modes is allowed while TO phonon scattering is forbidden in the (100) backscattering geometry. In the following, we discuss the Raman signal in these regions. In order to evaluate the wavenumbers of the different phonons contributing in this region of the Raman spectra, a curve fitting procedure was used (Lorentzian functions). Indeed, an example of line-shape fitting for sample PS1 in this range is presented in Fig. 10. The principal pic around (516.5 ± 0.1) cm^{-1} is allowed for the first-order longitudinal (LO) phonon mode of silicon (Si–Si) at the central point of the Brillouin zone (pink curve), which is a typical Raman profile as shown by Min yang et al. [19]. Other regions of Raman diffraction were observed: the first peak at (154 ± 14) cm^{-1} is the contribution of the first order for acoustical phonons TA(X) (green curve). The second at (298 ± 4) cm^{-1} is attributed to the longitudinal acoustic (LA) modes, however Iatsunsky et al. referred this peak to the second order of transverse acoustic phonons modes (2TA) (blue curve) [20, 21]. In addition, we can find a brad peak at (611 ± 7) cm^{-1}, which was associated to the quantum confinement effect of nano-crystallites silicon which were detected in dendritic structures: the combination of TO(X) + TA(X) mode (orange curve) [20]. Finally, (957 ± 1) cm^{-1} is assigned to the scattering of second-order transverse optical phonons ~ 2TO phonons (yellow curve) [22].

3.3.1 Pre-annealing

The Raman binding intensity is very sensitive to the structure of the sample, so fundamental information can be extracted from the intensity measurements: if we increase the layer thickness at a constant current density, the maximum of the most intense peak comes from the Si–Si phonon mode increase because we boost the surface area due to the matrix relaxation. It is known that the specific surface of porous silicon increases with the porosity rate. It is thus

Table 3 Peak separation in ω-2θ scan and the calculated perpendicular lattice strain in multilayer porous silicon (PSML) pre-and post-annealing treatment

Structures	θ_{Ps}	$\Delta\omega = \theta_{Si}$-$\theta_{Ps}$	$(\Delta d/d)$ $[10^{-4}]$
PSML1	34.574/34.551	-0.029/0.052	3.67/6.5
PSML2	34.581/34.554	-0.022/0.049	2.7/6.2
PSMLR1	34.430	-0.173	21.93
PSMLR2	34.449	-0.154	19.5

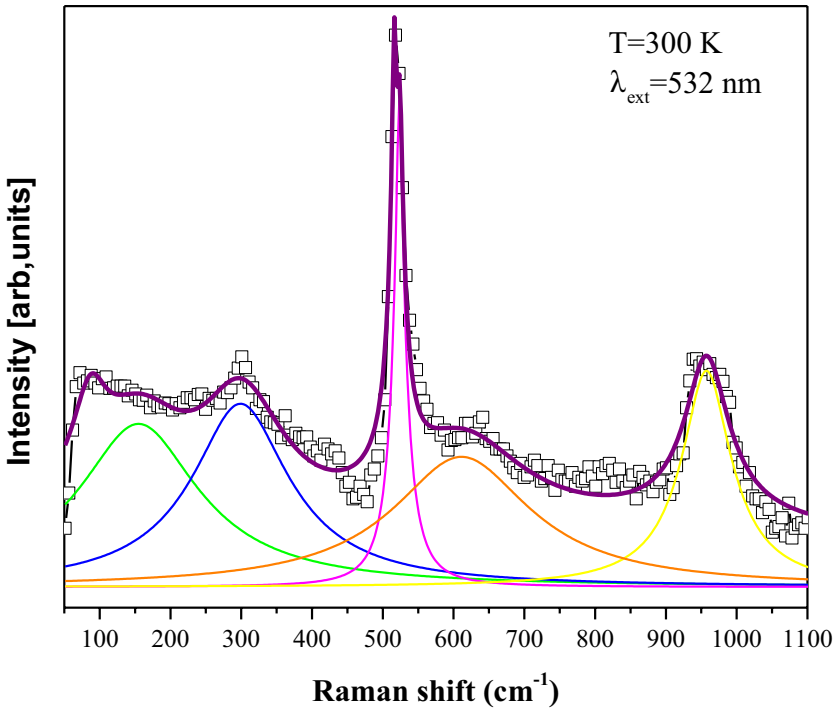

Fig. 10 Raman spectra of porous silicon monolayer PS1, recorded at room temperature with exciting wavelength $\lambda_{ext}=532$ nm

possible to create more effective influence on the surface Raman scattering [23].

For this reason, due to the development of the active-surface area, the peak intensity of the structure with highly porous thickness PS2 (PSML2) is more pronounced than PS1 (PSML1) as shown in Fig. 11, which is supported by Trusso et al. [24]; the main peak intensity at 520 cm^{-1} of the Raman scattering signal from porous silicon is enhanced by the increase of the interaction area due to the increase of the surface area. Other researchers attribute the scattering intensity to its proportionality to the equilibrium population and inelastic scattering cross-section of phonons [25]. Moreover, one of the most intriguing characteristics of the Raman spectrum is the sensitivity to the structural strain. Since the material is under strain, it may induce a negative or positive shift, either a tensile or a compressive strain. Figure 11 presents the evolution of the main Stokes scattering bands of the four structures after the anodizing process. Using the Lorentzian fit, it is clear that the Raman peak shifts towards lower energies (values smaller than 520 cm-^{1}: the typical value the of the silicon substrate (c-Si)). These negative shifts confirm the tensile stress that occurs in these structures due to relaxation process of the crystalline structure (Table 4). Therefore, we point out that the fabrication parameters (anodization time, current density….) affect the samples morphology, as we mentioned before in FE-SEM section. Experimental value reveals a fundamental dependence of Raman feature on strain (with respect to the c-Si) which is similar to Si associated with a decrease of crystallite sizes. In fact, an increase in current density implied an increase in the degree of porosity resulting an additional red shift of the optical phonon modes [26, 27].

Comparing PSML1 and PSML2, by following the comments (Fig. 12) of the thickness effect on the main peak intensity, we noticed a red shift towards lower energies. This behavior could be explained by the fact that the embedded gradual layers strongly influence the window layer.

This effect manifests for the sample with the thinner window layer thickness (PSML1). Regarding PSML2, this attitude is significantly less pronounced since PSML2 has the thickest top layer; in this case, the window layer of PSML2 sample will handle the deformation effect more than the one of PSML1. This outcome strengthens the results found by HR-XRD.

3.3.2 Upon Annealing

Previously, the HR-XRD measurement and FE-SEM analysis obtained during annealing in a non-oxidizing atmosphere confirmed a structural change. Table 1 (structures: PS2R and PSML2R) shows that during argon annealing, the size of the nanopores decreases. This attitude could be explained by the material expansion that leads to the pore's "closure". However, Dannefer et al. assigned this behavior to the gas oxidation that takes place due to the remaining air inside the pores of the film or adsorbed in the pore walls [28]. In our case, an oxidation could be occurred when samples were transferred to the HR-XRD chamber. Moreover, this decrease in size is due to sintering or coarsening of pores that exert a force on the crystallite.

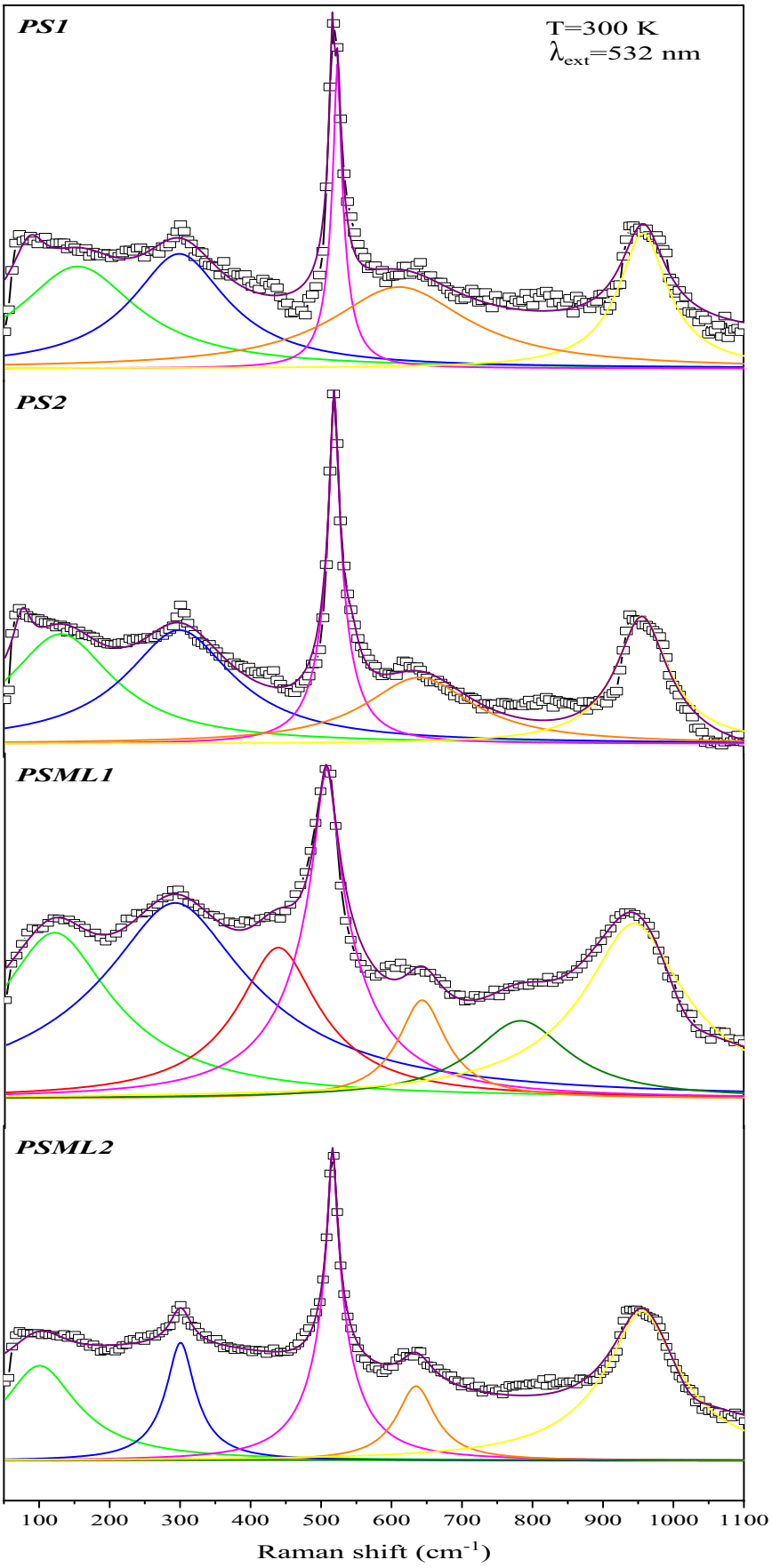

Fig. 11 Raman spectra of porous silicon recorded at room temperature with exciting wavelength $\lambda_{ext} = 532$ nm

Table 4 Experimental result of lattice constant perpendicular ($\Delta d/d$) and Lorentzian fit of the optical phonons at the central point of the Brillouin zone

Structures	ω (cm^{-1})	
	Pre-annealing	Post-annealing
PS1	516.50	518.42
PS2	518.84	517.94
PSML1	506.69	517.87
PSML2	518.85	514.87

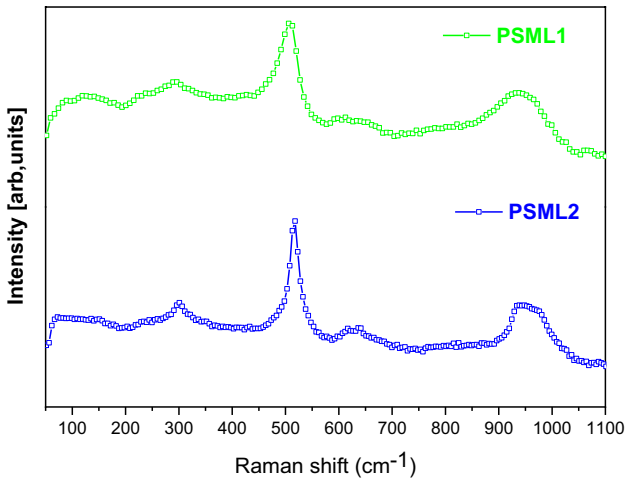

Fig. 12 Raman spectra of porous silicon multilayer PSML1, PSML2 recorded at room temperature with exciting wavelength $\lambda_{ext} = 532$ nm

Figure 13 shows a slight red shift with respect to the porous scattering which is due to the decrease of crystal symmetry originated from size reduction of silicon nanocrystals within the porous matrix [29]. Since the annealing treatment boosts the pores migration from the top layer towards the substrate interface, the window layer deformation will be less noticeable after annealing for both structures PS2R and PSML2R. However, the effect of the three gradual layers on the deformation of the top layer will be low as long as the transferable volume of pores is almost identical (according to MEB observations). In terms of intensity, the main peak of PSML2R is more intense (inset figure) because the surface of the pores is much more significant.

4 Conclusion

In this work, we have evaluated the interest of using porous silicon and thermal annealing in order to modulate the window layer strain, which it will allow a defect-free epitaxial growth of lattice mismatch materials. As a first step, we have elaborated a monolayer porous structure (PS) with two different thicknesses, then three gradual porous layers were created underneath each PS structures; which triggers a porosity gradient, hence the origin of the stress modification in the window layer. The last approach was to study the annealing effect that was carried out under argon gas at 900 °C. This investigation highlighted the pores migration phenomenon, therefore the stress modification. Regarding the PS samples, as FE-SEM measurement revealed, increasing

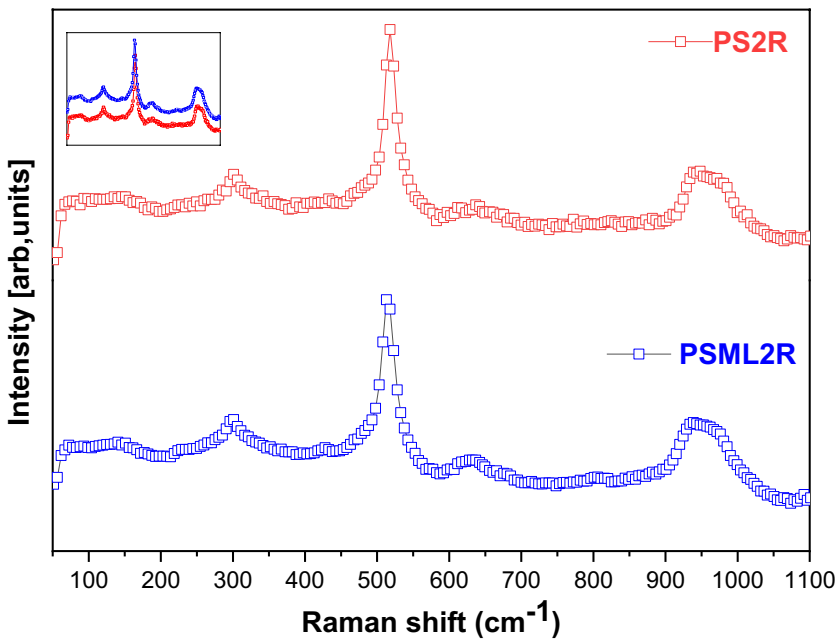

Fig. 13 Raman spectra of multilayer porous silicon PSML2, PS2R recorded at room temperature with exciting wavelength $\lambda_{ext} = 532$ nm

the anodization time increases the porous silicon thickness at constant current densities. HR-XRD analysis showed that perpendicular strain farther increases which implies an expansion in lattice parameter with respect to the substrate. Such a behavior was detected for PSML structures but with important strain evolution, which emphasizes the indirect effect induced by the bottom layers (HPLs) on the window layer. The top porous layers were morphologically affected under heat treatment. This process was intended to reorganize pores within each structure: the PS FE-SEM top view showed a radical change in pores geometry by sealing them to create a quasi-monocrystalline layer, while the embedded pores undergo a coalescence due to sintering. This microstructural change leads to an additional perpendicular strain manifested by a red shift in HR-XRD profiles. A similar attitude was observed for PSMLs specimens where Ostwald ripening process occurs in the bottom porous layers. Besides to the morphological results and HR-XRD investigations, Nano-Raman spectra allowed a well comprehension of the mechanism occurs in those structures: with a Lorentzian fit and regarding the phonon mode of the central point of the Brillouin zone, we have affirmed that the increase of the main peak intensity witnessed the proportionality of the rate expansion of the Si–Si bonds. It is important to mention that for the thickest window layer the contribution to the increase of the peak intensities is dominant as shown in FE-SEM images. Thus, the structures with higher window layer thicknesses (PS2 and PSML2) acquired a significant intensity. Due to its sensitivity to strain, the negative shift verified the tensile strain detected in HR-XRD profiles. The additional shift confirmed also the significant contribution of these incorporated layers.

Acknowledgements We gratefully thank Ahmed Benmanaa, Technical Support Manager at LaboServices, for his contribution in HR-XRD analysis.

Author Contributions - Imen Zeydi: Validation/ visualization/ writing -original draft/ writing-review and editing - Aicha Saidi: Investigation/ Validation/ visualization/ writing -original draft/ writing-review and editing - Badreddine Smiri: Editing - Isabelle Berbezier: Resourses - Ridha Mghaieth: Supervision.

Data Availability The authors confirm that the data of this study are available within the article.

Declarations

Ethics Approval Not applicable.

Consent to Participate Not applicable.

Consent for Publication The author confirms:

- That the work has been approved by all co-authors;
- That the work described has not been published before;
- That is not under consideration for publication elsewhere.

Competing Interests The authors declare no competing interests.

References

1. Lyshevski SE (2018) Nano- and Micro-Electromechanical Systems: Fundamentals of Nano-and Microengineering, 2nd ed., CRC Press. https://doi.org/10.1201/9781315219288
2. Artmann H, Schaefer F, Lammel G, Armbruster S, Benzel H, Schelling C, Weber H, Vossenberg H-G, Gampp R, Muchow J (2003) Monocrystalline Si membranes for pressure sensors fabricated by a novel surface-micromachining process using porous silicon, in: MEMS Compon. Appl. Ind. Automob. Aerosp. Commun. II, SPIE. pp. 65–70
3. Knese K, Armbruster S, Weber H, Fischer M, Benzel H, Metz M, Seidel H (2009) Novel Technology for Capacitive Pressure Sensors with Monocrystalline Silicon Membranes, in: 2009 IEEE 22nd Int. Conf. Micro Electro Mech. Syst. pp. 697–700. https://doi.org/10.1109/MEMSYS.2009.4805478
4. Al-Jumaili BEB, Al-Jumaili BEB, Talib ZA (2016) Photoelectric properties of Metal-Semiconductor-Metal Photodetector based on Porous Silicon. J. Solid St. Sci. & Technol. Letters. 17:79–82
5. Al-Jumaili B, Talib ZA, Ramizy A, Aljameel A, Baqiah H, Ahmed NM, Paiman SB, Liew JYC, Lee HK (2021) Formation and photoluminescence properties OF porous silicon/copper oxide nanocomposites fabricated via electrochemical deposition technique for photodetector application. Dig J Nanomater Biostruct. 16:297–310
6. Azeza B, Sfaxi L, M'ghaieth R, Fouzri A, Maaref H (2011) Growth of n-GaAs layer on a rough surface of p-Si substrate by molecular beam epitaxy (MBE) for photovoltaic applications. J Cryst Growth. 317:104–109
7. Chiang C-C, Lee BT-H (2019) Annihilating Pores in the Desired Layer of a Porous Silicon Bilayer with Different Porosities for Layer Transfer. Sci Rep 9:12631. https://doi.org/10.1038/s41598-019-49119-8
8. Riikonen J, Salomäki M, van Wonderen J, Kemell M, Xu W, Korhonen O, Ritala M, MacMillan F, Salonen J, Lehto V-P (2012) Surface Chemistry, Reactivity, and Pore Structure of Porous Silicon Oxidized by Various Methods. Langmuir 28:10573–10583. https://doi.org/10.1021/la301642w
9. Rahmani N, Dariani RS (2016) Effect of porous silicon buffer under different porosities on lateral overgrowth of TiO2 nanorods on silicon substrate. J Alloys Compd 681:421–425. https://doi.org/10.1016/j.jallcom.2016.04.234
10. Martini R, SivaramakrishnanRadhakrishnan H, Depauw V, Van Nieuwenhuysen K, Gordon I, Gonzalez M, Poortmans J (2013) Improvement of seed layer smoothness for epitaxial growth on porous silicon. Mrs Proc. 1536:97–102. https://doi.org/10.1557/opl.2013.748
11. Sivaramakrishnan Radhakrishnan H, Martini R, Depauw V, Van Nieuwenhuysen K, Debucquoy M, Govaerts J, Gordon I, Mertens R, Poortmans J (2014) Improving the Quality of Epitaxial Foils Produced Using a Porous Silicon-based Layer Transfer Process for High-Efficiency Thin-Film Crystalline Silicon Solar Cells. IEEE J. Photovolt 4. https://doi.org/10.1109/JPHOTOV.2013.2282740
12. Solanki CS, Bilyalov RR, Poortmans J, Beaucarne G, Van Nieuwenhuysen K, Nijs J, Mertens R (2004) Characterization of free-standing thin crystalline films on porous silicon for solar cells. Thin Solid Films 451–452:649–654. https://doi.org/10.1016/j.tsf.2003.11.157
13. Young IM, Beale MIJ, Benjamin JD (1985) X-ray double crystal diffraction study of porous silicon. Appl Phys Lett 46:1133–1135. https://doi.org/10.1063/1.95733
14. Karim M, Martini R, Radhakrishnan HS, van Nieuwenhuysen K, Depauw V, Ramadan W, Gordon I, Poortmans J (2014) Tuning of strain and surface roughness of porous silicon layers for higher-quality seeds for epitaxial growth. Nanoscale Res Lett 9:348. https://doi.org/10.1186/1556-276X-9-348

15. Labunov V, Bondarenko V, Glinenko I, Dorofeev A, Tabulina L (1986) Heat treatment effect on porous silicon. Thin Solid Films 137:123–134. https://doi.org/10.1016/0040-6090(86)90200-2
16. Barla K, Herino R, Bomchil G, Pfister JC, Freund A (1984) Determination of lattice parameter and elastic properties of porous silicon by X-ray diffraction. J Cryst Growth 68:727–732. https://doi.org/10.1016/0022-0248(84)90111-8
17. Abramof PG, Beloto AF, Ueta AY, Ferreira NG (2006) X-ray investigation of nanostructured stain-etched porous silicon. J Appl Phys 99:024304. https://doi.org/10.1063/1.2162273
18. Maehama TMT, Afuso CAC, Itoh NIN (1998) Structural Analysis of Porous Silicon Multilayer using X-Ray Diffraction. Jpn J Appl Phys 37:998. https://doi.org/10.1143/JJAP.37.998
19. Yang M, Huang D, Hao P, Zhang F, Hou X, Wang X (1994) Study of the Raman peak shift and the linewidth of light-emitting porous silicon. J Appl Phys 75:651–653. https://doi.org/10.1063/1.355808
20. Iatsunskyi I, Jurga S, Smyntyna V, Pavlenko M, Myndrul V, Zaleska A (2014) Raman spectroscopy of nanostructured silicon fabricated by metal-assisted chemical etching, in. https://doi.org/10.1117/12.2051489
21. Wei W (2007) One- and two-phonon Raman scattering from hydrogenated nanocrystalline silicon films. Vacuum 81:857–865. https://doi.org/10.1016/j.vacuum.2006.10.005
22. Kravets VG, Kolmykova VYu (2005) Raman scattering of light in silicon nanostructures: First-and second-order spectra. Opt Spectrosc 99:68–73. https://doi.org/10.1134/1.1999895
23. Lin G-R, Lin Y-H, Pai Y-H, Meng F-S (2011) Si nanorod length dependent surface Raman scattering linewidth broadening and peak shift. Opt Express 19:597–605. https://doi.org/10.1364/OE.19.000597
24. Trusso S, Vasi C, Allegrini M, Fuso F, Pennelli G (1999) Micro-Raman study of free-standing porous silicon samples. J Vac Sci Technol B Microelectron Nanometer Struct Process Meas Phenom 17:468–473. https://doi.org/10.1116/1.590578
25. Periasamy S, Sasirekha V, Ragavendran V, Mayandi J, Pearce J, Selj J, Veerabahu R (2017) Micro-Raman Scattering of Nanoscale Silicon in Amorphous and Porous Silicon. Z Für Phys Chem 231. https://doi.org/10.1515/zpch-2016-0961
26. Smerdov RS, Spivak YM, Levitsky VS, Moshnikov VA (2018) The characterisation of nanostructured porous silicon/silver layers via Raman spectroscopy. J Phys Conf Ser 1038:012064. https://doi.org/10.1088/1742-6596/1038/1/012064
27. Campbell IH, Fauchet PM (1986) The effects of microcrystal size and shape on the one phonon Raman spectra of crystalline semiconductors. Solid State Commun 58:739–741. https://doi.org/10.1016/0038-1098(86)90513-2
28. Dannefaer S, Wiebe C, Kerr D (1998) Positron annihilation investigation of porous silicon heat treated to 1000 °C. J Appl Phys 84:6559–6564. https://doi.org/10.1063/1.369028
29. Bouzourâa MB, Rahmani M, Zaïbi M-A, Lorrain N, Haji L, Oueslati M (2013) Optical study of annealed cobalt-porous silicon nanocomposites. J Lumin 143:521–525. https://doi.org/10.1016/j.jlumin.2013.05.050